



Integrated sensor with a whispering-gallery mode and surface plasmonic resonance for the enhanced detection of viruses

YIHUA HAO AND ZHIXIONG GUO*

Department of Mechanical and Aerospace Engineering, Rutgers, The State University of New Jersey, Piscataway, New Jersey 08854, USA

*Corresponding author: zguo@rutgers.edu

Received 4 March 2021; accepted 23 August 2021; posted 26 August 2021 (Doc. ID 424250); published 13 September 2021

Surface plasmonic resonance (SPR) is integrated into a whispering-gallery mode (WGM) optical microsensor to augment sensitivity in this study. The performance of such WGM silica ring sensors of 20 μm in size with an Ag or Au metal core was evaluated for detection of small respiratory viruses such as COVID-19 via the finite-element modeling. Compared with pure WGM sensors, the integration with SPR enhances sensitivity by 3–5 times and facilitates combination with the polymerase chain reaction method to achieve fast, accurate, and specific virus detection. The presence of a single respiratory virus of 70 to 100 nm in diameter in air environment could shift the sensor resonance wavelength by 36 to 64 pm in the case of an Au metal core or by 34 to 63 pm of an Ag metal core. With use of a general-purpose optical analyzer of 10 pm resolution, a single airborne virus of 20 nm in size is detectable using the proposed hybrid sensor. This corresponds to about 0.005 vol. %. For viruses in aqueous solution, the detection limit rises to about 0.2 vol. %. A fundamental enhancement factor based on relative electric energy ratio is introduced and defined to analyze and quantify sensitivity enhancement for the first time, to the best of our knowledge. © 2021 Optical Society of America

<https://doi.org/10.1364/JOSAB.424250>

1. INTRODUCTION

In recent years, some respiratory diseases have significantly impacted public health safety [1]. Respiratory viruses that have been identified and contained include severe acute respiratory syndrome coronavirus (SARS), influenza A, influenza B, and H1N1. In 2020, the spread of COVID-19 had caused a severe disaster for human beings, and we are living in challenging times. Therefore, it is urgently needed to develop responding biosensors to meet the needs of rapid and accurate detection, effectively preventing the spread of the virus, reducing medical expenses, and helping relevant agencies control the pandemic [2].

Optical whispering-gallery mode (WGM) resonators have excellent characteristics of high Q -factor and small mode volume [3]. WGM sensors have been extensively investigated in many fields, e.g., temperature measurement [4], gas detection [5], force/pressure measurement [6], and magnetic field measurement [7]. Light circulates many times in a WGM resonator due to the total internal reflection (TIR), resulting in extremely high Q -factor. Similarly, the interaction between the evanescent field and the surrounding target/matter is enhanced, showing incredible potentials in biological sensing applications [8,9]. Utilizing a WGM resonator as a biosensor for label-free and highly sensitive nanoparticles [10–12] and biolayer detection [13] has proven feasible. Among them, single virus detection,

as a technology, allows us to detect at low concentration, identify the size and type of the virus quickly, and study further the physical, chemical, and biological characteristics of the virus [14]. However, it is noticed that the traditional WGM microsensors with a diameter of less than 100 μm have a low sensitivity for detecting single nano-entities [15]. Enhancing sensitivity can significantly improve the feasibility of the device in real applications.

From the reactive sensing principle [16] for WGM sensors for detection of a nanoparticle, the fractional frequency shift $\Delta\omega_r/\omega_r$ is

$$\frac{\Delta\omega_r}{\omega_r} = -\frac{\Delta\lambda_r}{\lambda_r} = -\frac{W_p}{W_c} \cong -\frac{\alpha_{\text{ex}}|E_0(r_v)|^2}{2\int \varepsilon_c |E_0(r)|^2 dV}, \quad (1)$$

where W_p is the energy required to polarize the particle under detection, W_c is the energy in the cavity, α_{ex} is the excess polarizability of a nanoparticle, ε_c is the permittivity of the resonator, $E_0(r_v)$ is the modal field amplitude of the target nanoparticle at radial position r_v , and $E_0(r)$ is the modal field amplitude throughout the mode. For an individual micro-resonator, enhancing the detective position's electric field intensity can increase the wavelength (frequency) shift, thereby increasing the sensitivity.

Surface plasmon resonance (SPR) technology has become an indispensable part of biomolecular detection [17,18]. Same as WGM's TIR principle, when a beam of light illuminates the SPR coupler's boundary and is internally reflected, it will form an evanescent field on the coupler's surface. Hence, it provides a prerequisite for the combination of the two technologies. Several recent studies have found that WGM can be combined with SPR to enhance the sensor's sensitivity [19,20] effectively. Besides, the widely used real-time reverse transcription-polymerase chain reaction (RT-PCR) method for COVID-19 detection [21] can be directly integrated on an SPR gene chip to achieve a higher diagnostic accuracy rate, specification, and functionality [22].

In this study, we propose a hybrid sensor that combines WGM and SPR technologies to enhance virus detection. The hypothesis is that the SPR greatly enhances the WGM ring resonator electric field intensity in the detection regime and, thus, the sensitivity. It could be combined with the RT-PCR method to achieve fast and accurate detection of respiratory viruses. Through intensive finite-element modeling, it is demonstrated that the proposed biosensor can detect the presence of a single airborne virus. The enhancement of sensitivity is analyzed and quantified. An enhancement factor based on the relative electric energy ratio is defined and introduced; this factor matches the frequency shift enhancement ratio very well. This research provides a promising new vision for rapid respiratory virus detection as well as a new theoretical foundation for sensitivity enhancement.

2. MODEL AND SIMULATION

The exciting laser for both the WGM and SPR waves is governed by Maxwell's equations, which are simplified to the Helmholtz equation:

$$\frac{1}{\mu} \nabla^2 \bar{E} + \omega^2 \varepsilon_c \bar{E} = 0, \quad (2)$$

where \bar{E} is the electric field vector, the complex permittivity is $\varepsilon_c = \varepsilon - i(\sigma/\omega)$, and the angular frequency of the wave is $\omega = 2\pi c/\lambda$, in which c is the speed of light in vacuum and λ is the exciting wavelength. ε and σ are the permittivity and conductivity of the medium, respectively. The complex permittivity can also be related to the refractive index n and the absorption index k [23] as follows:

$$\varepsilon_c = n^2 - k^2 - i2nk. \quad (3)$$

In the present simulation, the in-plane TE mode is assumed. The electromagnetic waves only propagate in the $x - y$ plane. The scattering boundary condition is applied to both the optical waveguide and ring resonator side to ensure that the boundary is entirely transparent for scattered waves and any angle of incident waves in the 2D plane.

The schematic of the proposed hybrid device is sketched in Fig. 1, where the silicon wafer substrate that does not participate in the reaction is ignored. The WGM ring resonator and waveguide are placed in the air domain. The side length W_s is 1.5 times the ring resonator diameter D_1 to ensure that all optical components that need to be simulated are included. The

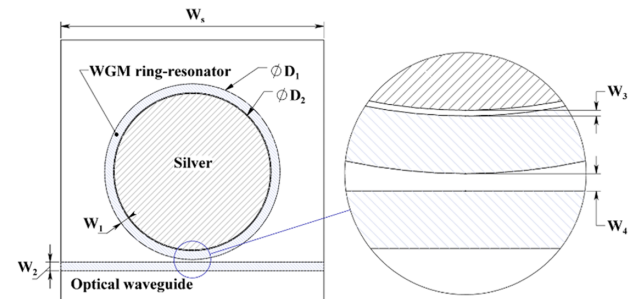


Fig. 1. Schematic of the hybrid biosensor.

refractive index of air is approximated as $n_{\text{air}} = 1$. We chose silica as the optical WGM ring resonator material in the present study because of its low material loss, low cost, and extensive practical applications. It has been proven that silica WGM resonators have an ultra-high Q factor [24]. The refractive index of silica used in the present modeling is $n_{\text{silica}} = 1.44507$ at 300 K [25]. A tunable laser as the light source is injected from the optical waveguide's left side inlet. The exciting wavelength is around 1550 nm. The loss of this band in silica is low. The ring resonator thickness W_1 varies from 1 μm to 1.5 μm , and the optical waveguide thickness W_2 is 1 μm to ensure that optical waves penetrate the boundary, resulting in WGM phenomena [9,26].

The noble metal core is a co-centered micro-disk inside the WGM ring resonator. The core and the ring resonator are separated by a sensing gap W_3 . Two common metal materials to generate SPR, i.e., silver (Ag) and gold (Au), are considered and compared. The relative permittivity of silver is $\{\varepsilon_1, \varepsilon_2\} = \{-120.17, 3.067\}$ at 1550 nm, where ε_1 and ε_2 are the real part and imaginary part, respectively. The relative permittivity of gold is $\{\varepsilon_1, \varepsilon_2\} = \{-115.13, 11.259\}$ at 1550 nm [27]. Since the size of most respiratory viruses is in the range of 70–100 nm and a single COVID-19 virus is about 70–90 nm [28,29], the sensing gap in the present study is designed as $W_3 = 120$ nm if not otherwise specified. The exciting light coupling gap W_4 is the distance between the optical waveguide and the WGM ring resonator. Previous work has proved an optimal gap distance W_4 for achieving maximum light energy transfer and storage [30]. The refractive index of biological viruses is assumed to be the same as that of protein bovine serum album (BSA), i.e., $n_{\text{virus}} = 1.5$ [31]. The geometric parameters and optical properties are summarized in Tables 1 and 2, respectively.

We used commercial software COMSOL 5.4 to simulate the performance of the proposed hybrid biosensor. The meshing of the simulation domain consists of unstructured triangular meshes. Previous results of layered deposition detection showed that when the maximum element size in the meshing was less than 1/8 wavelength, the computational error was less than 5% [30]. Figure 2 examines the computational convergence for this study, in which the maximum electric field and the maximum element size, as well as the wavelength shift caused by the presence of a single virus of 70 nm in diameter versus the element number used in simulation, were plotted. Other important parameters include exciting wavelength at 1550 nm, $D_1 = 20 \mu\text{m}$, $W_3 = 120$ nm, and use of Ag metal core. As shown in Fig. 2(a), the maximum element size was decreased

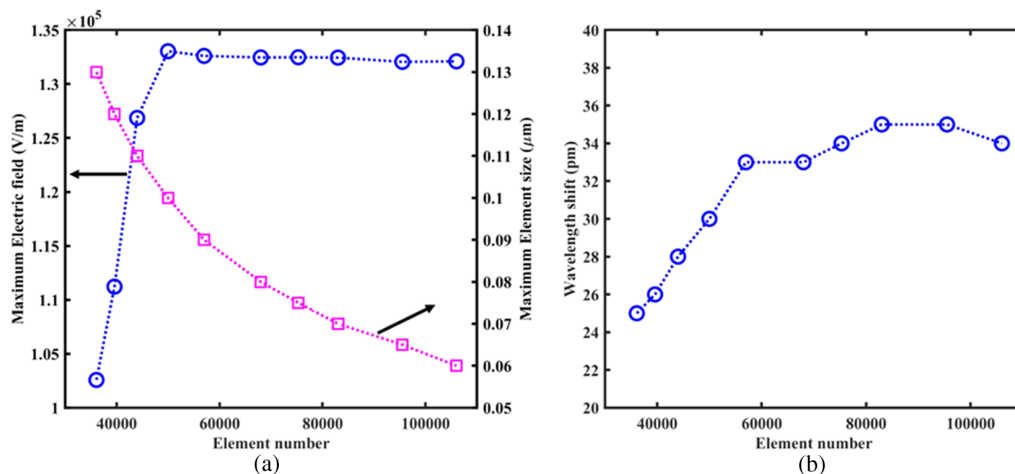


Fig. 2. Convergence check in simulation: (a) maximum electric field intensity and maximum element size versus element number; (b) wavelength shift versus element number.

Table 1. Geometric Parameters

Parameter	Definition	Value
D_1	Diameter of the ring resonator	20 [μm]
D_2	Diameter of the SPR metal core	17.6–17.9 [μm]
W_1	Ring resonator thickness	1–1.5 [μm]
W_2	Optical waveguide thickness	1 [μm]
W_3	Sensing gap distance	50–200 [nm]
W_4	Coupling gap distance	300 [nm]
W_s	Side length of the air domain	30 [μm]

Table 2. Optical Properties

Parameter	Definition	Value
n_{air}	Refractive index of air	1
n_{silica}	Refractive index of silica	1.44507
n_{virus}	Refractive index of virus	1.5
n_{water}	Refractive index of water	1.33
ϵ_1	Relative permittivity of Ag/Au (real part)	-120.17/-115.13
ϵ_2	Relative permittivity of Ag/Au (imaginary part)	3.067/11.259

from 130 nm to 60 nm when the element number was increased from 36,000 to 106,000. When the element number reaches 75,000 in the present study, i.e., when the maximum element size is about 75 nm ($\sim 1/20$ wavelength), both the calculations in E-field and wavelength shift converge, with an error of 1% in the maximum E-field and of 3% in the induced wavelength shift. Hence, such a meshing size is adopted in all the calculations thereafter. To find a resonance shift with a resolution to

1 pm, it took about 2 hr CPU time when using a Lenovo PC with i7-6700 CPU at 3.4 GHz and 16 GB RAM.

3. RESULTS AND DISCUSSION

According to the reactive sensing principle, the sensitivity of a WGM sensor is determined by the energy ratio between the polarization of the target and the resonance cavity. Therefore, it can be enhanced by increasing the electric field intensity in the detection area and/or reducing the electric field throughout the resonator. Figure 3 compares the electric field intensity distributions along the radial direction for different sensor structures using either Ag or Au as the SPR core material or without the use of a metal core. In the five cases studied in the figure, the outer diameter and the thickness of the ring resonator keep constant, i.e., $D_1 = 20 \mu\text{m}$ and $W_1 = 1 \mu\text{m}$. The gap between the WGM ring and the SPR core filled with air is 50 nm in Fig. 3(a) and 120 nm in Fig. 3(b), and correspondingly the SPR core diameter D_2 is either 17.9 μm or 17.76 μm . With an Ag or Au core, both SPR and WGM occur. In the case without a SPR core marked as “Pure,” it is purely a WGM ring resonator in an air environment; thus, the same “Pure” curve is shown Figs. 3(a) and 3(b). The sensing gap is a tiny region to the left-hand side of the dashed line at radial position of 9 μm . Since the imaginary part $\epsilon_2 (= 11.259)$ in gold’s relative permittivity is much larger than that of silver ($= 3.067$), it is seen that the electromagnetic waves attenuate much more for the cases with an Au core. However, the electric field in the sensing gap with a gold core is higher than that inside the ring. The ratio between the sensing regime’s average electric field intensity of the hybrid structure and pure resonator is 2.09 (Ag) and 0.84 (Au) in Fig. 3(a), and 1.75 (Ag) and 1.0 (Au) in Fig. 3(b). Although the electric field in the sensing area for the two cases with an Au core is not enhanced in comparison with the case without a metal core, the electric field in the WGM resonator with an Au core is substantially reduced, which will inversely increase the sensitivity. For a pure ring resonator, it is observed that the ratio between the average electric field intensity in the sensing region and that in the resonator is 0.65. With the presence of a metal core, however, it is

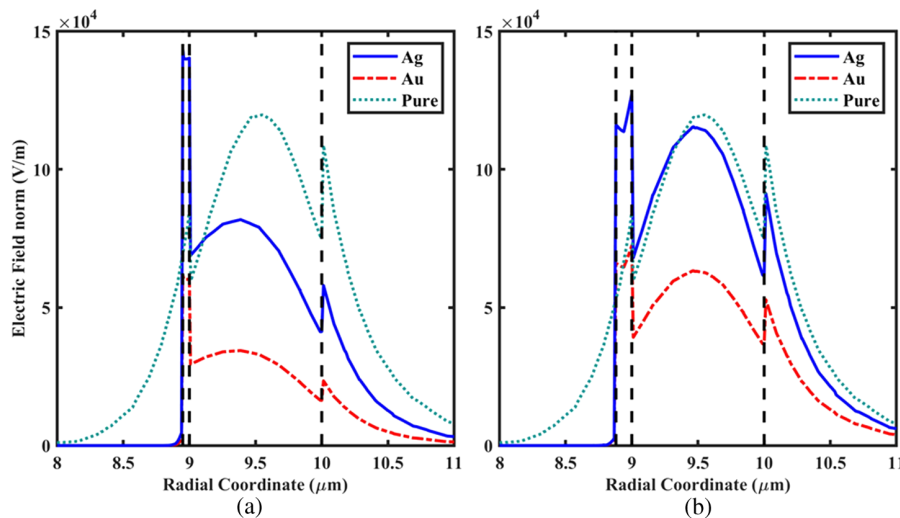


Fig. 3. Electric field intensity distributions without virus presence of (a) a 50 nm sensing gap and (b) a 120 nm sensing gap.

clearly seen that such a ratio is increased, about 2.0 with an Ag core and 2.03 with an Au core in Fig. 3(a), and 1.23 (Ag) and 1.25(Au) in Fig. 3(b), respectively. This ratio determines if the sensitivity of the WGM sensor and the ratio values for the Ag and Au cores are similar. Both metals can be deployed as the SPR core with similar enhancement ratio. In actual applications, gold's physical and chemical stability is much better than that of silver [32], but gold is also much more expensive. Hence, both materials are considered in this work.

The energy transported by a wave is directly proportional to the square of the amplitude of the electric field, i.e., $|E|^2$. Consider the ratio relationship in Eq. (1): a 2D circular model is simplified as

$$\frac{\Delta\lambda_r}{\lambda_r} = \frac{\alpha_{ex} |\overline{E}_p|^2}{2\varepsilon_c \int (2\pi r |E_0(r)|^2) dr}. \quad (4)$$

\overline{E}_p is the average electric field intensity of the target, and $E_0(r)$ is the electric field intensity distribution throughout the ring resonator mode. Here we propose a new parameter, the enhancement factor F , as follows:

$$F = \frac{|\overline{E}'_p|^2}{|E_p|^2} \left(\frac{\int (r |E_0(r)|^2 dr)}{\int (r |E'_0(r)|^2 dr)} \right), \quad (5)$$

where the E-field symbols with an apostrophe represent values with an SPR core while those without mean a pure WGM ring resonator. Thus, the enhancement factor theoretically indicates the WGM sensitivity's enhancement ratio due to the use of an SPR core.

Figure 4 shows the effect of the sensing gap on the enhancement factor F with a sensing gap W_3 varying from 80 nm to 200 nm for both the Ag and Au cores. The ring resonator thickness is 1 μm , and the target detection is a virus of 70 nm in diameter located 5 nm away from the inner side of the ring resonator. It is seen that the enhancement factor F decreases as the sensing gap enlarges. The maximum enhancement factor F in the study range is 4.8/5.0 at 80 nm sensing gap corresponding to the Ag/Au core, and the minimum F is 2.5/2.6 at 200 nm

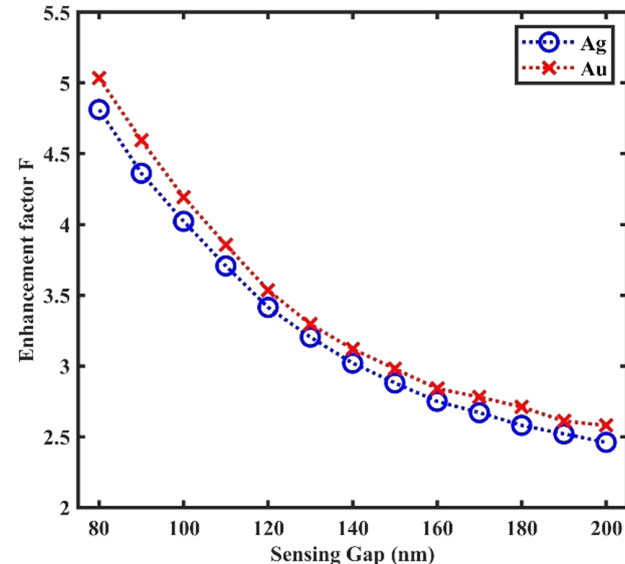


Fig. 4. Enhancement factor versus sensing gap distance.

sensing gap. Since the general size of most respiratory viruses is in the range of 70–100 nm, the sensing gap in the present study is designed as $W_3 = 120$ nm if not otherwise specified. At this gap value, the enhancement factor is 3.4 for Ag core and 3.5 for Au core, respectively. The results of the simulation with viruses of different sizes will not obviously affect the value of F . The sensitivity enhancement ratio is close between the Ag and Au cores, though the Au core performs slightly better.

Another critical parameter that determines the performance of a WGM optical sensor is the Q -factor of the resonator, defined as

$$Q = \frac{\omega_0}{\Delta\omega} = \frac{f_0}{\Delta f}, \quad (6)$$

in which $f_0 = \omega_0/2\pi$ is the resonance frequency and Δf is the full width at half-maximum (FWHM) of a resonance band. The Q -factor limits the resolution of a WGM sensor [33]. The simulated Q -factor of a pure silica ring resonator of

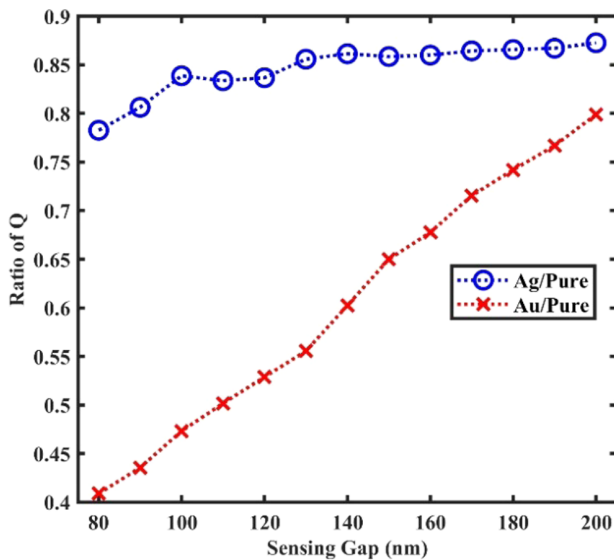


Fig. 5. Ratio of Q -factor versus sensing gap.

$\{D_1, W_1\} = \{20 \mu\text{m}, 1 \mu\text{m}\}$ is 3520. Since part of the photon energy stored in the ring participates in the SPR reaction, the introduction of an SPR core reduces the electric field intensity in the WGM resonator as shown in Fig. 3; thus, the Q -factor for the hybrid sensor is smaller than that of a pure ring resonator. Figure 5 shows the ratio of Q -factor between the hybrid sensor and the pure ring resonator. With increasing sensing gap distance, the Q -factor of the hybrid sensor increases. At the designated sensing gap of 120 nm, the Q -factor ratio is 0.84 with an Ag core and 0.53 with an Au core, respectively. The Au metal core lowers the Q -factor more than the Ag metal core. Although the Q -factor is somewhat sacrificed due to using a metal core, the sensitivity enhancement is more significant as discussed in Fig. 4.

Figure 6 examines the effect of the ring resonator thickness on both the enhancement factor F and the Q -factor ratio. The sensing gap between the WGM ring of 20 μm in diameter and the metal core is 120 nm with a single virus of 70 nm in size. With increasing ring thickness, the Q -factor increases as more energy can be confined inside the ring, but the enhancement

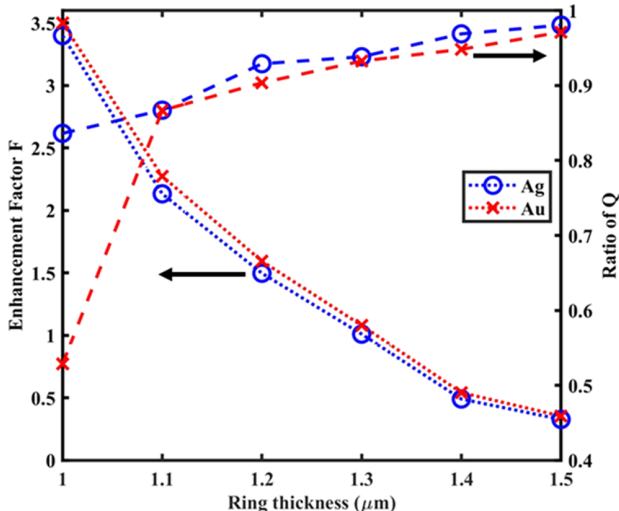


Fig. 6. Effect of ring resonator thickness.

factor reduces because less energy can get out of the WGM ring to generate SPR. When the ring thickness is over 1.3 μm , the enhancement factor is less than unity, i.e., no enhancement. Since this study focuses on sensitivity enhancement, a ring thickness of 1 μm is selected if not otherwise mentioned.

When a virus (assumed as an effective spherical nanoparticle) enters the sensing gap of the integrated sensor, a change in resonance wavelength (also known as the wavelength/frequency shift) is induced. Figure 7 shows and compares the spectra with or without a single virus of 70 nm in diameter. The SPR metal core is made of Ag. It is measured that the single virus leads to a resonance wavelength shift by 34 pm, a value that is large enough to be detectable with a general-purpose optical analyzer. We further altered the location of the single virus in the sensing gap, and results showed nearly unchanged wavelength shift; in other words, the shift is insensitive to the virus position in the sensing gap.

Figure 8 shows the size effect of a single virus on the wavelength shift and the enhancement ratio of wavelength shifts between the hybrid WGM/SPR and pure WGM sensors. As shown in Fig. 8(a), the induced wavelength shift increases with increasing virus size. Respiratory viruses usually have a size ranging from 70 nm to 100 nm in diameter and result in a wavelength shift from 36 pm to 64 pm for the Au core and from 34 pm to 61 pm for the Ag core. Such shifts are much larger than that caused by a pure silica WGM ring sensor without a metal core, demonstrating the enhancement of sensitivity due to the use of a metal core. With the use of a general-purpose optical analyzer of 10 pm resolution, the minimum detectable virus size is around 20 nm in diameter, corresponding to a volume concentration of about 0.005%. As shown in Fig. 8(b), the sensitivity enhancement ratio, i.e., the ratio of wavelength shifts with and without a metal core, scatters slightly with varying virus sizes. Nevertheless, the average sensitivity enhancement ratio is 3.35 ± 0.16 for the Au core and 3.08 ± 0.14 for the Ag core. These two results are in close agreement with the values of the enhancement factor F based on the relative electric energy ratio, which were 3.5 and 3.4, respectively. It fully proved the accuracy of our modeling and theoretical analysis, indicating that the enhancement factor obtained from the electric field distribution can be used to analyze the sensitivity enhancement. The induced wavelength shift is determined by the ratio of electric energy between the target and the WGM resonator. The presence of an SPR core will intensify this electric energy ratio and, thus, will lead to sensitivity enhancement.

In actual operations, viruses may exist in aqueous solution, and there may exist multiple viruses binding to the metal core due to electrical charges. Since viruses have zeta potential [34], the positive and negative charges of the metal core can be adjusted by intervening micro currents to make different types of viruses adsorb onto the metal core, enabling specification and functionality during detection. The scenario with binding of multiple viruses is converted to virus volume concentration and displayed in Fig. 9, in which the viruses are in aqueous solution, rather than airborne as studied in the afore single virus cases. The aqueous solution will put on more challenges as the contrast of electric properties between the gap environment and the WGM ring medium reduces. Certainly, it would be better to use

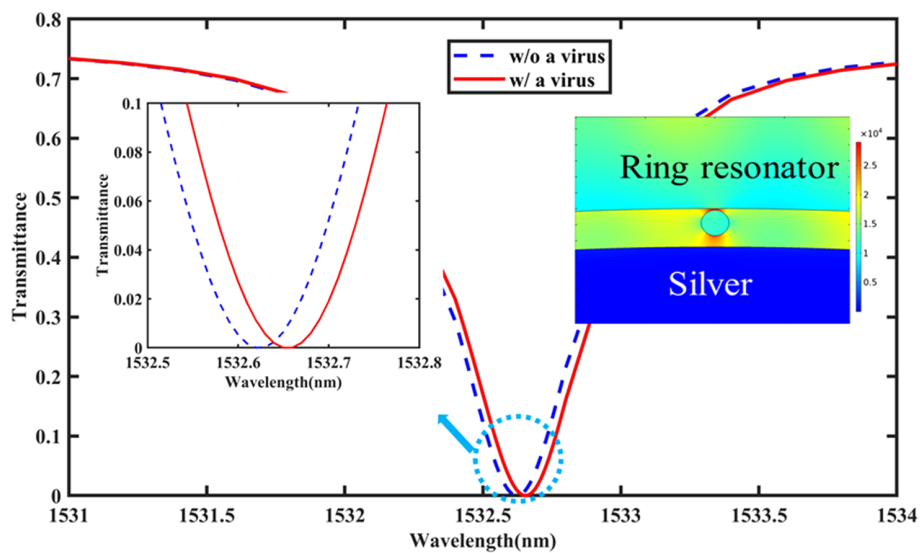


Fig. 7. Detection of wavelength shift due to the presence of a single virus of 70 nm in diameter.

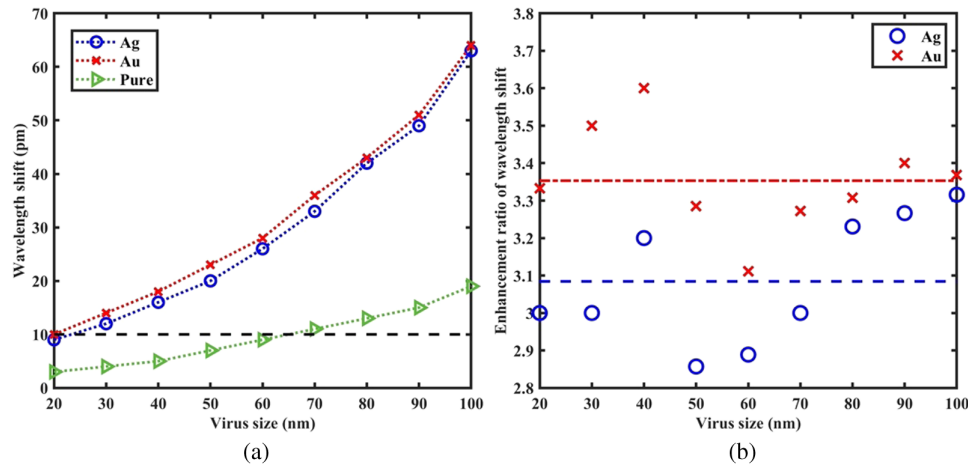


Fig. 8. (a) Wavelength shift versus the size of a single virus and (b) enhancement ratio of wavelength shift.

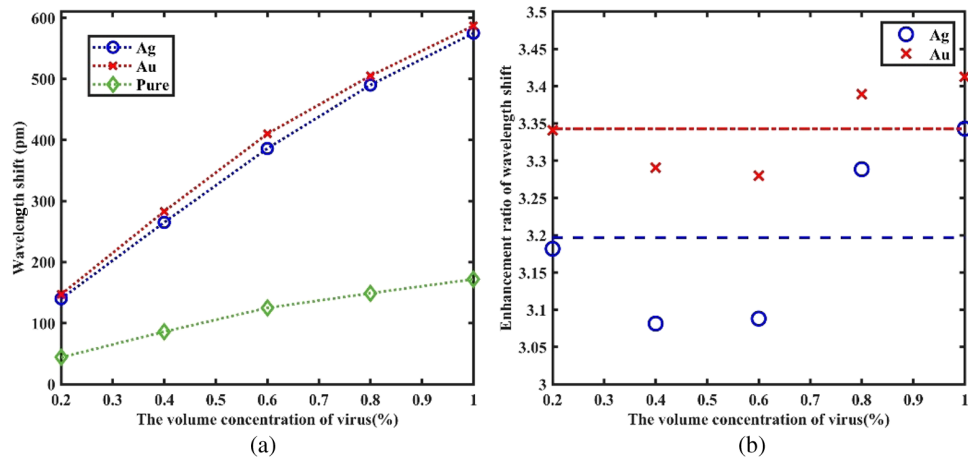


Fig. 9. (a) Wavelength shift and (b) enhancement ratio of wavelength shift versus virus concentration in aqueous solution.

higher refractive ring material such as silicon or silicon nitride, which will be investigated in our next work.

In the present simulation, the refractive indices of the water and virus layer are assumed as 1.33 and 1.50, respectively. As shown in Fig. 9(a), a range of volume concentration of virus from 0.2% to 1% will induce a wavelength shift from 147 pm to 587 pm for the gold core hybrid sensor or 140 pm to 575 pm for the silver core sensor. The induced shifts with an SPR core are much larger than the pure WGM ring sensor. The Q -factor with aqueous gap here is reduced to 1260 for the gold core and 1840 for the silver core. With reduction in both Q -factor and contrast of optical constants between water and virus, virus detection with volume concentration below 0.2% becomes unstable in our simulation. The enhancement factor F is calculated as 3.5 (Au) and 3.4 (Ag) with a sensing gap of 120 nm, respectively. Same as the afore single airborne virus study, it is found that the volume concentration in aqueous solution will not obviously affect the value of the F -factor. From Fig. 9(b), it is seen that the average shift sensitivity enhancement ratio is 3.34 ± 0.06 for the Au core and 3.2 ± 0.12 for the Ag core, closely matching with their F -factor values.

4. CONCLUSION

This paper aimed to investigate the enhancement of WGM sensitivity with the addition of SPR and demonstrate ultra-sensitivity and feasibility of the hybrid optical sensor in detecting a single respiratory virus for rapid test response to the pandemic. Both silver and gold metal cores could be used to generate the SPR, and their enhancement factor values were close. Although the silver core increased but the gold core reduced the electric field intensity in the sensing target, it was found that the most important parameter that affected the sensitivity of the WGM sensor was the ratio of the electric field in the target to that in the WGM resonator. An enhancement factor F was introduced and defined as the ratio between the stored electric energy in the target to that in the WGM resonator. It was found that this F -factor value was in close agreement with the ratio of the induced wavelength shifts between a WGM/SPR hybrid sensor and a pure WGM sensor. The results revealed the sensitivity enhancement magnitude as well as the theoretical mechanism for detection enhancement for the first time. The addition of an SPR metal core inside a WGM ring resonator would generally enhance the WGM sensitivity by 3–5 times in the present cases studied.

Various hybrid sensor structures were compared. The effects of the sensing gap, ring resonator thickness, and virus size were scrutinized. In the present study, the exciting optical wavelength was around 1.5 μm , and the diameter of the silica WGM ring was fixed at 20 μm with varying ring thickness from 1 to 1.5 μm and varying sensing gap from 80 to 200 nm, under the presence of a respiratory virus that is usually 70–100 nm in size. It was found that with reducing ring thickness, enhancement F -factor increased, but the Q -factor in the WGM resonator reduced. The enhancement on F is much stronger than the reduction in Q . With decreasing the sensing gap, the F -factor increased but Q -factor reduced. The effects of ring thickness and sensing gap on the Q -factor with an Au core were severer than those with an Ag core. But their effects on the F -factor were similar

between the Au and Ag cores. For the designed sensor structure $\{D_1, W_1, W_3\} = \{20 \mu\text{m}, 1 \mu\text{m}, 120 \text{ nm}\}$, the enhancement factor F was calculated as 3.4 of an Ag core and 3.5 of an Au core in the detection of a single virus. Corresponding to a respiratory virus of 70–100 nm in size in the airborne environment, the wavelength shift was from 34 to 61 pm with an Ag metal core and 36 to 64 pm with an Au metal core, easily detectable via a general-purpose optical analyzer. The minimum detectable size is around 20 nm in diameter, corresponding to a volume concentration of 0.005%. Compared to a pure WGM ring resonator, the enhancement ratio in wavelength shift is 3.08 ± 0.14 for the Ag core and 3.35 ± 0.16 for the Au core. Only a minor difference exists between the enhancement ratio in real wavelength shift and the theoretical enhancement F -factor. Further, the value of the F -factor was found not to be influenced by the virus size. Therefore, the F -factor would be a very useful parameter to understand and quantify sensitivity enhancement.

Detection of viruses in aqueous solution is more challenging as the contrast of optical properties among the target, the gap, and the present WGM ring medium becomes smaller. Indeed, we may use a higher refractive ring medium to mitigate the concern, which is under study. In the aqueous scenario of the present study, the enhancement factor F was found to be 3.5 of Au and 3.4 of Ag metal core, respectively, closely matching with the wavelength shift enhancement ratio 3.34 ± 0.06 for the Au core and 3.2 ± 0.12 for the Ag core. The detection limit for virus in aqueous solution was found to be around 0.2 vol. %. This research provides a promising new vision for rapid respiratory virus detection as well as a new theoretical foundation for optical WGM sensitivity enhancement.

Disclosures. The authors declare no conflicts of interest.

Data Availability. Data underlying the results presented in this paper are not publicly available at this time but may be obtained from the authors upon reasonable request.

REFERENCES

1. T. Ferkol and D. Schraufnagel, "The global burden of respiratory disease," *Ann. Am. Thorac. Soc.* **11**, 404–406 (2014).
2. Y. Amano and Q. Cheng, "Detection of influenza virus: traditional approaches and development of biosensors," *Anal. Bioanal. Chem.* **381**, 156–164 (2005).
3. M. L. Gorodetsky, A. A. Savchenkov, and V. S. Ilchenko, "Ultimate Q of optical microsphere resonators," *Opt. Lett.* **21**, 453–455 (1996).
4. Y. Hao and Z. Guo, "Monitor *in situ* superconducting temperature via optical whispering-gallery mode sensors," *J. Phys. D* **52**, 175101 (2019).
5. Y. Sun and X. Fan, "Analysis of ring resonators for chemical vapor sensor development," *Opt. Express* **16**, 10254–10268 (2008).
6. T. Ioppolo and M. V. Ötügen, "Pressure tuning of whispering gallery mode resonators," *J. Opt. Soc. Am. B* **24**, 2721–2726 (2007).
7. A. Mahmood, V. Kavungal, S. S. Ahmed, G. Farrell, and Y. Semenova, "Magnetic-field sensor based on whispering gallery modes in a photonic crystal fiber infiltrated with magnetic fluid," *Opt. Lett.* **40**, 4983–4986 (2015).
8. H. Zhu, P. S. Dale, C. W. Caldwell, and X. Fan, "Rapid and label-free detection of breast cancer biomarker CA15-3 in clinical human serum samples with optofluidic ring resonator sensors," *Anal. Chem.* **81**, 9858–9865 (2009).
9. H. Quan and Z. Guo, "Simulation of whispering-gallery-mode resonance shifts for optical miniature biosensors," *J. Quant. Spectrosc. Radiat. Transfer* **93**, 231–243 (2005).

10. H. Quan and Z. Guo, "Simulation of single transparent molecule interaction with an optical microcavity," *Nanotechnology* **18**, 375702 (2007).
11. A. M. Armani, R. P. Kulkarni, S. E. Fraser, R. C. Flagan, and K. J. Vahala, "Label-free, single-molecule detection with optical microcavities," *Science* **317**, 783–787 (2007).
12. F. Vollmer and S. Arnold, "Whispering-gallery-mode biosensing: label-free detection down to single molecules," *Nat. Methods* **5**, 591–596 (2008).
13. M. Noto, F. Vollmer, D. Keng, I. Teraoka, and S. Arnold, "Nanolayer characterization through wavelength multiplexing of a microsphere resonator," *Opt. Lett.* **30**, 510–512 (2005).
14. F. Vollmer, S. Arnold, and D. Keng, "Single virus detection from the reactive shift of a whispering-gallery mode," *Proc. Natl. Acad. Sci. USA* **105**, 20701–20704 (2008).
15. A. Bozzola, S. Perotto, and F. De Angelis, "Hybrid plasmonic–photonic whispering gallery mode resonators for sensing: a critical review," *Analyst* **142**, 883–898 (2017).
16. S. Arnold, M. Khoshima, I. Teraoka, S. Holler, and F. Vollmer, "Shift of whispering-gallery modes in microspheres by protein adsorption," *Opt. Lett.* **28**, 272–274 (2003).
17. K. M. Mayer and J. H. Hafner, "Localized surface plasmon resonance sensors," *Chem. Rev.* **111**, 3828–3857 (2011).
18. P. Zijlstra, P. M. Paulo, and M. Orrit, "Optical detection of single non-absorbing molecules using the surface plasmon resonance of a gold nanorod," *Nat. Nanotechnol.* **7**, 379–382 (2012).
19. S. Shopova, R. Rajmangal, S. Holler, and S. Arnold, "Plasmonic enhancement of a whispering-gallery-mode biosensor for single nanoparticle detection," *Appl. Phys. Lett.* **98**, 243104 (2011).
20. J. D. Swaim, J. Knittel, and W. P. Bowen, "Detection limits in whispering gallery biosensors with plasmonic enhancement," *Appl. Phys. Lett.* **99**, 243109 (2011).
21. L. Lan, D. Xu, G. Ye, C. Xia, S. Wang, Y. Li, and H. Xu, "Positive RT-PCR test results in patients recovered from COVID-19," *J. Am. Med. Assoc.* **323**, 1502–1503 (2020).
22. F. Watzinger, K. Ebner, and T. Lion, "Detection and monitoring of virus infections by real-time PCR," *Mol. Aspects Med.* **27**, 254–298 (2006).
23. B. E. Saleh and M. C. Teich, *Fundamentals of Photonics* (Wiley, 2019).
24. T. Kippenberg, S. Spillane, D. Armani, and K. Vahala, "Fabrication and coupling to planar high-Q silica disk microcavities," *Appl. Phys. Lett.* **83**, 797–799 (2003).
25. D. B. Leviton and B. J. Frey, "Temperature-dependent absolute refractive index measurements of synthetic fused silica," *Proc. SPIE* **6273**, 62732K (2006).
26. I. M. White, H. Oveys, and X. Fan, "Liquid-core optical ring-resonator sensors," *Opt. Lett.* **31**, 1319–1321 (2006).
27. P. B. Johnson and R.-W. Christy, "Optical constants of the noble metals," *Phys. Rev. B* **6**, 4370–4379 (1972).
28. J.-M. Kim, Y.-S. Chung, H. J. Jo, N.-J. Lee, M. S. Kim, S. H. Woo, S. Park, J. W. Kim, H. M. Kim, and M.-G. Han, "Identification of coronavirus isolated from a patient in Korea with COVID-19," *Osong Publ. Health Res. Perspect.* **11**, 3–7 (2020).
29. S. Wang, X. Shan, U. Patel, X. Huang, J. Lu, J. Li, and N. Tao, "Label-free imaging, detection, and mass measurement of single viruses by surface plasmon resonance," *Proc. Natl. Acad. Sci. USA* **107**, 16028–16032 (2010).
30. Z. Guo, H. Quan, and S. Pau, "Near-field gap effects on small microcavity whispering-gallery mode resonators," *J. Phys. D* **39**, 5133–5136 (2006).
31. K. Yeung, Z. Lu, and N. Cheung, "Adsorption of bovine serum albumin on fused silica: elucidation of protein–protein interactions by single-molecule fluorescence microscopy," *Colloids Surf. B* **69**, 246–250 (2009).
32. K. E. Lee, A. V. Hesketh, and T. L. Kelly, "Chemical stability and degradation mechanisms of triangular Ag, Ag@Au, and Au nanoprisms," *Phys. Chem. Chem. Phys.* **16**, 12407–12414 (2014).
33. Q. Ma, T. Rossmann, and Z. Guo, "Whispering-gallery mode silica microsensors for cryogenic to room temperature measurement," *Meas. Sci. Technol.* **21**, 025310 (2010).
34. J. Vajda, D. Weber, S. Stefaniak, B. Hundt, T. Rathfelder, and E. Müller, "Mono- and polyprotic buffer systems in anion exchange chromatography of influenza virus particles," *J. Chromatogr. A* **1448**, 73–80 (2016).